RESEARCH ARTICLE

Investigation on modeling parameters of concrete beams reinforced with basalt FRP bars

Jordan CARTER, Aikaterini S. GENIKOMSOU[*]

Civil Engineering Department, Queen's University, Kingston, ON K7N 3N6, Canada
[*]*Corresponding author. E-mail: ag176@queensu.ca*

ABSTRACT   Fiber-reinforced polymer (FRP) bars are widely used as internal reinforcement replacing the conventional steel bars to prevent from corrosion. Among the different types of FRP bars, basalt FRP (BFRP) bars have been used in different structural applications and, herein, three already tested concrete beams reinforced with BFRP bars are analyzed using three-dimensional (3-D) finite element analysis (FEA). The beams were tested in four-point bending. In the FEA the behavior of concrete is simulated using the "Concrete-Damaged Plasticity" model offered in ABAQUS software. The research presented here presents a calibrated model for nonlinear FEA of BFRP concrete beams to predict their response considering both the accuracy and the computational efficiency. The calibration process showed that the concrete model should be regularized using a mesh-dependent characteristic length and material-dependent post-yield fracture and crushing energies to provide accurate mesh-size independent results. FEA results were compared to the test results with regard to failure load and crack patterns. Both the test results and the numerical results were compared to the design predictions of ACI 440.1R-15 and CSA S806-12, where CSA S806-12 seems to overestimate the shear strength for two beams.

KEYWORDS   basalt Fiber-reinforced polymer bars, reinforced concrete beams, finite element analysis, damaged plasticity model, design codes

1   Introduction

Fiber-reinforced polymers (FRPs) are often considered to replace conventional steel since they are thermally insulating, corrosion resistant in saline environments, non-ferrous, and have a much lower weight than steel. Many times, these advantages are associated with the decrease in stiffness and the increase in expense of working with FRPs. However, as FRPs become a more common and mature technology, this cost is decreasing rapidly. In general, FRP reinforcing bars are characterized by a high tensile strength, little to no yielding before failure, corrosion resistance, a low modulus of elasticity, and low shear strength [1]. Glass fiber reinforced polymer (GFRP) and carbon fiber reinforced polymer (CFRP) are the most common choices for FRP reinforcement, however, aramid FRP (AFRP) can be another option. The newest option that has become available is basalt FRP

(BFRP). Basalt fibers were invented in 1923, however, they were classified for military use until recently with BFRP rebar became available around 2007, meaning they are rarely used in civilian applications [2]. BFRP is currently categorized according to Ref. [1] as a type of natural fiberglass fiber. The limited use of BFRP in structures is often attributed to the recent availability of the material and associated lack of governance and regulation. BFRP typically has a failure stress of approximately twice that of a similar sized steel reinforcement bar with the modulus of elasticity being about one fifth that of steel [3]. Additionally, like most other FRPs, BFRP has a linear stress strain relationship with little to no yielding before failure. Ultimately BFRP is a promising replacement for GFRP as it is stronger and has a higher stiffness, while being price competitive with glass fibers.

Recently, many researchers considered testing reinforced concrete beams using BFRP bars as internal reinforcement [4–6]. The findings of their research predicted that the shear strength of BFRP reinforced

concrete beams is in good agreement with the shear behavior of concrete beams reinforced with other types of FRP bars. In that sense, finite element analysis (FEA) can be considered to supplement the experimental data and perform parametric studies to further investigate the behavior of concrete beams reinforced with BFRP bars. The FEA analyses are integrated using the software ABAQUS [7] with the "Concrete Damaged Plasticity" (CDP) model that considers isotropic damage elasticity combined with isotropic tensile and compressive plasticity to represent the inelastic behavior of concrete. CDP model considers a combined non-associated multi-hardening plasticity and isotropic damage elasticity to describe the damage that occurs during fracture. A fracture energy cracking model [8] can be used to specify the post-failure tensile stress as a tabular function of cracking displacement.

The main objective of this paper is to describe how calibration process is performed in FEA of concrete beams. The calibrated models can be used for future parametric studies to investigate how certain design parameters affect the flexural and the shear strength of the BFRP beams. Calibrated FEA can be helpful for developing future design codes of BFRP beams. In this research, the calibration study examines the constitutive model for concrete where the comparison between simulated and measured responses showed that the concrete model should be regularized using a mesh-dependent characteristic length and material-dependent post-yield fracture and crushing energies to provide accurate mesh-size independent results. Selected beams were previously tested [4] are herein considered for the numerical investigation. One of the tested and analyzed beams, denoted as NT, was considered as the reference beam to calibrate the FEA model. NT did not have shear reinforcement, while the other two beams, denoted as FT and FC, had stirrups, but differed in the amount of flexural reinforcement they contained. All beams had as longitudinal and transverse reinforcement BFRP bars. Further calibration was considered to model the confined concrete for the beams reinforced with stirrups. Finally, the design equations according to ACI 440.1R-15 [1] and CSA S806-12 [9] are presented and the design predictions are compared to both the test results and the numerical results.

2   Test specimens

The test series consist of nine beams that vary in the amount of flexural reinforcement and the type of shear reinforcement they contain. Each beam underwent a deflection controlled 4-point bending test at a deflection rate of 2 mm per minute until failure. The beams were supported at each end by a steel roller beneath a 12.7 mm thick, 152 mm by 152 mm steel plate. These supports were separated by 2900 mm. A similar arrangement was used to

apply the load evenly to both sides of the beam. A single stiff hollow steel section was used to apply the loads 350 mm to either side of the center-point. The loads were transferred through rollers and then through 150 mm by 100 mm steel plates to the beam. Deflections were measured at 5 points using linear potentiometers (LPs), at the center of the beam, at 550 mm from each support and at 1200 mm from each support. A visualization of the test set-up can be seen in Fig. 1. Three beams were selected to be analyzed in ABAQUS. All beams are rectangular with a cross-section 150 mm × 300 mm and 3100 mm long. One of the tested beams (NT) was considered as the reference beam to calibrate the FEA model. NT did not have shear reinforcement, while the other two selected beams FT and FC had stirrups only in the shear zone, however, they differed in the amount of flexural reinforcement. Figure 2 presents the cross-sections of the beams with the longitudinal and transverse BFRP reinforcement. The clear concrete cover is equal to 20 mm.
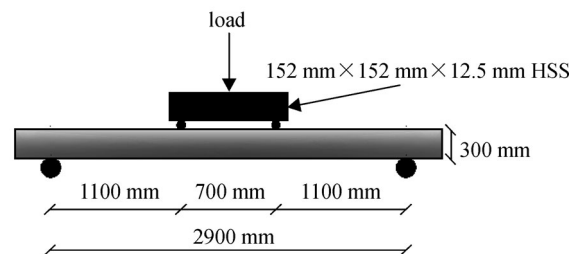

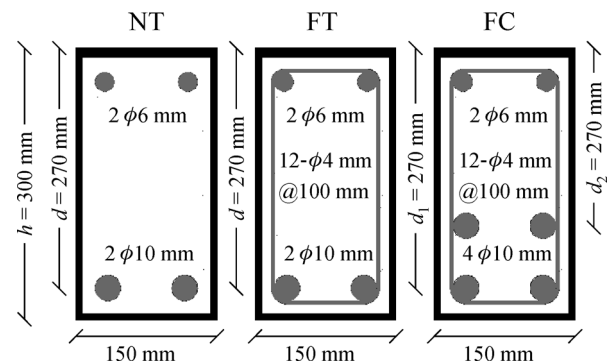**Fig. 1**   Schematic drawing of test apparatus.

Fig. 2   Schematic drawing of the beams (cross-sections).

The material properties of the beams and the test results are shown in Tables 1 and 2, respectively. All specimen failed in shear: NT beam showed two shear cracks in both sides of the compressive zone, FT beam achieved its peak load and immediately its stirrups near the corners ruptured and FC beam showed shear crush in the compression zone at peak load followed by rupture of the stirrups near the corners. Figure 3 shows the test results of the beams in terms of load versus mid-span deflection and Fig. 4

Table 1 Material properties of the beams

beam	concrete				BFRP bars/stirrups		
	f'_c (MPa)	f'_t (MPa)	G_f (N/mm)	E_c (MPa)	f_y (MPa)	E_s (MPa)	A_s (mm^2)
NT	60.0	2.6	0.138	38730	1100	70000	157
FT	51.0	2.4	0.126	35707	1100	70000	157
FC	52.1	2.4	0.127	36090	1100	70000	314

Note: f'_c = cylinder compressive strength of concrete (calculated from tests); f'_t = tensile strength of concrete = $0.33\sqrt{f'_c}$; G_f= fracture energy of concrete (CEB fib Model Code 90 10), aggregate size 19 mm; E_c= modulus of elasticity of concrete = $5000\sqrt{f'_c}$; f_y= yield stress of BFRP bars and stirrups; E_s= modulus of elasticity of BFRP bars and stirrups; A_s= cross-sectional area of bottom BFRP bars.

Table 2 Test results

beam	stirrups	depth, d (mm)	reinforcement ratio, ρ	failure load (kN)	failure displacement (mm)	failure mode
NT	No	270	0.0039	41.8	95.8	shear (tension)
FT	BFRP	270	0.0039	72.7	59.8	shear (stirrup rupture)
FC	BFRP	245	0.0085	106.9	61.6	shear (stirrup rupture)
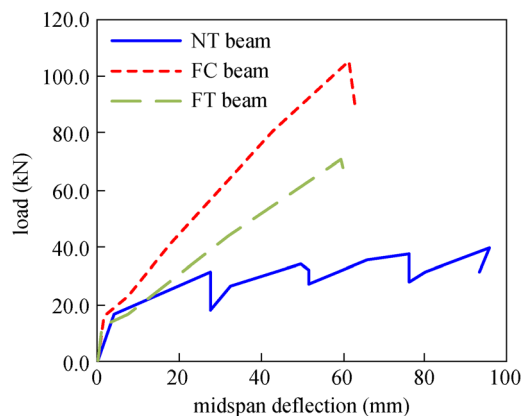
Fig. 3 Load versus mid-span deflection curves of the tested beams.

illustrates the crack patterns of the beams according to the test results.

3 FEA

FEA of reinforced concrete structures consider advanced constitutive models with concepts of plasticity, damage, and coupled damage-plasticity to model the complex behavior of concrete. Classical plasticity models [11–13] many times cannot capture the stiffness degradation of concrete under cyclic loading. Thus, damage mechanics models were developed to simulate the stiffness degradation using the effective stresses [14–17]. A combination of plasticity and damage in coupled damage-plasticity models can model the deterioration, the permanent deformation and volumetric expansion of concrete [18–22].

In the present research, a combined damage-plasticity model (CDP) is considered for all analyses. CDP model was first developed by Lubliner et al. [21] and later

modified by Lee and Fenves [22]. CDP can be considered when concrete is subjected to monotonic, cyclic and/or dynamic loading under low confining pressure. It combines non-associated multi-hardening plasticity and isotropic damaged elasticity to describe the irreversible damage that happens during the fracturing process and controls the stiffness recovery during cyclic loading. CDP model uses the non-associated Drucker-Prager hyperbolic function as the flow potential function, G, which is defined according to Eq. (1).

$$G = \sqrt{(\varepsilon\sigma_{to}\tan\psi)^2 + \overline{q}^2} - \overline{p}\tan\psi, \qquad (1)$$

where ε is the eccentricity which defines the rate of approximation between the plastic potential function and the asymptote, σ_{to} is the biaxial tensile stress, and ψ is the dilation angle measured in the p-q plane at high confining pressure. In the current analyses dilation is considered equal to 36° according to ABAQUS manual. The plastic strain increment is normal to the plastic potential function and the default value for the eccentricity is 0.1 displaying that the dilation angle of concrete does not change. The dilation angle shows the direction of the plastic strain increment vector [23].

For the current shear tests of the beams the definition of the damage parameters can be omitted since damage parameters are important for cyclic and/or dynamic loadings where unloading is defined by means of plastic strain. Table 3 presents the plasticity parameters that should be defined in ABAQUS, where K_c parameter determines the shape of the yield surface. According to ABAQUS manual the value of the K_c parameter should range between 0.5 and 1 with a default value equal to 0.667. The viscous parameter (μ) can be defined to upgrade the plastic strain tensor by providing additional relaxation time to the model. Quasi-static analysis under displacement control is conducted in ABAQUS/Explicit
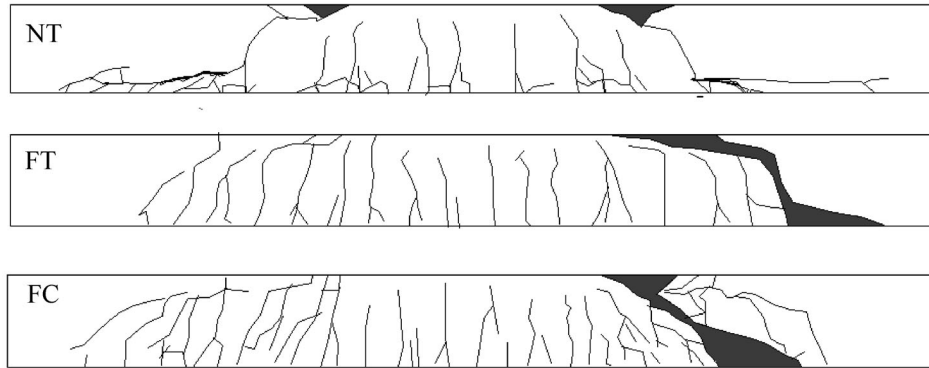
Fig. 4   Crack patterns of the tested beams.

Table 3   Plasticity properties of concrete for the beams

parameter	value
dilation angle ψ	36°
ε	0.1
$\dfrac{\sigma_{bo}}{\sigma_{co}}$	1.16
K_c	0.667
μ	0

Table 4   BFRP material properties

Young's Modulus (MPa)	Poisson's ratio	yield stress (MPa)
70000	0.22	1100

roller and pin supports to be introduced at the bottom of the edges.

3.1   Calibration of FEA model

Beam NT contained no stirrups and was considered as the control specimen for the calibration procedure. During this process different mesh sizes and plasticity parameters were investigated to achieve a reasonable agreement with the test results and then use the calibrated model to analyze the other two beams. Quasi-static analysis under displacement control is used in ABAQUS/Explicit. Concrete is modeled with three-dimensional (3-D) 8-noded hexahedral elements with reduced integration (C3D8R) and the flexural reinforcement is modeled with 3-D 2-noded linear truss elements (T3D2). When truss elements model the reinforcement, the concrete behavior is considered independently and effects associated with the reinforcement/concrete interface, such as bond slip and dowel action, are modeled approximately by introducing some "tension stiffening" into the concrete modeling to simulate load transfer across cracks through the rebar. Thus, perfect bond between concrete and reinforcement through the embedded method is assumed. The bilinear tension stiffening response of concrete proposed by Hillerborg et al. [8] is considered: at the stress $f_t'/3$, the crack displacement is equal to $0.8G_f/f_t'$ and then, when the stress is zero the cracking displacement is equal to $3.6G_f/f_t'$. The fracture energy of concrete (G_f) that represents the area under the tensile stress-crack width curve is considered and it is calculated according to Eq. (2) based on CEB-FIP Model Code 1990 [10]:

$$G_f = G_{fo}(f_{cm}/f_{cmo})^{0.7}, \tag{2}$$

since it requires less computational time compared to the static analysis in ABAQUS/Standard and does not consider viscoplastic regularization (μ) that may be a hard task to be defined.

In compression the response of concrete is linear until the initial yield stress and then is characterized by stress hardening first and then by strain softening beyond the ultimate stress. In tension, the concrete stress-strain curve is linear elastic until the failure stress. At this failure stress, the micro-cracking in concrete starts. Beyond the failure stress, micro-cracking is presented macroscopically with a stress-strain softening response that prompts strain localization in concrete.

Reinforcement of concrete structures is modeled with truss elements embedded into concrete. Bond slip is considered indirectly in a simple manner by introducing tension stiffening, which allows to define the strain-softening behavior for cracked concrete. Tension stiffening can be modeled using the fracture energy cracking criterion [24]. Thus, the brittle behavior of concrete is characterized by a stress-displacement response instead of a stress-strain response.

The uniaxial stress-strain relation of BFRP reinforcement was modeled as elastic with Young's modulus (E_s) and Poisson's ratio (v). Table 4 presents the material properties of the BFRP reinforcement (longitudinal and transverse).

Regarding the geometry and the boundary conditions of the analyzed beams, the whole beams are modeled with

where $f_{cmo} = 10$ MPa, f_{cm} is the mean value of the compressive strength associated with the characteristic compressive strength f_{ck}, $f_{cm} = f_{ck} + 8$ MPa, and G_{fo} is the base fracture energy that depends on the maximum aggregate size, d_{max}. The value of the base fracture energy G_{fo} for the 19 mm aggregate size of the tested beams was calculated equal to 0.035 N/mm. The Hognestad-type parabola was considered to model the compressive behavior of the concrete beams. Figures 5(a) and 5(b) present the stress-strain and the stress-inelastic strain behavior (input data) of concrete beam NT, respectively.

3.1.1 Tension stiffening

In reinforced concrete members under tensile load, cracks form and open when concrete reaches its tensile strength. The developed shear forces at the contact surface develop tension stresses into the concrete between the cracks. Concrete hangs on the bar and contributes to the overall stiffness of the member. This effect is called tension stiffening and can be accounted for in an indirect way by assuming that the loss of tension strength in concrete appears gradually. Tension stiffening was first introduced by Scanlon [25] and later by Bergan and Holand [26]. To investigate the effect of tension stiffening in the response of the control specimen NT three different values for the fracture energy were considered. The calculated fracture energy $G_f = 0.138$ N/mm was increased to account for more tension stiffening (0.15 and 0.2 N/mm) and also decreased to 0.12 N/mm. It should be noted that in the numerical analyses presented in this section, a mesh size equal to 25 mm is assumed. A mesh size sensitivity analysis is presented in the next section. Figure 6 shows the tensile stress versus crack width curves for the four different values of fracture energy that were considered as inputs for the tensile behavior of concrete. Based on the FEA results, Fig. 7 presents the load-deflection responses for beam NT for all four given values of fracture energy. The numerical results obtained by using different values for the fracture energy show that the contribution of the

tensile behavior to the response of the beam is significant. Regarding the visualization of cracking, the concrete damaged plasticity model assumes that cracking initiates at points where the tensile equivalent plastic strain is greater than zero and the maximum principal plastic strain is positive. Based on the load-deflection responses and by comparing the numerical results with the failure load of the tested NT beam, it was concluded that the fracture energy should be considered equal to 0.138 N/mm as it was calculated using the equations form CEB fib Model Code 90. This value is considered for all the following analyses to calibrate the concrete model of the beam NT. Figure 8 shows the cracking through the tensile equivalent plastic strains (PEEQT) for the fracture energy $G_f = 0.138$ N/mm. Large diagonal shear cracks, similar to those seen in the real tests, were observed in the analysis. In the real test the diagonal shear crack developed when the mid-span deflection reached 28 mm. Around the load that caused the initial failure, a second large shear crack opened up on the other side of the beam. As the beam deflected further, failure observed in both sides and new peaks achieved till the final failure. Similar response observed in the FEA where after the initial failure, a second large shear crack appeared at 40 mm and dropped the load. Then new peaks achieved and the final failure appeared in a similar manner with the test at 100 mm.

3.1.2 Mesh size sensitivity analysis

The impact of mesh size on the FEA response of the control beam was also examined. The smeared crack approach considered in the FEA, creates strain localization within only few elements and the rest of the structure starts to unload. Finer mesh leads to narrow band of localization and the numerical equations fail to converge [22]. For this reason, the model becomes mesh size dependent as do most plasticity models that exhibit strain softening. This issue can be solved by using mesh regularization techniques, such as the introduction of the characteristic internal crack length through the softening portion of the stress-strain relationship of the constitutive model. One of
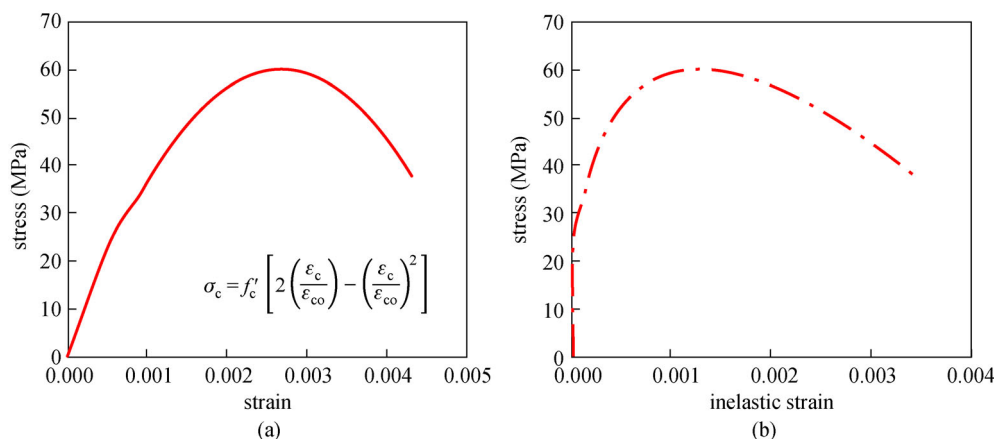

Fig. 5 Compressive behavior of concrete: (a) stress-strain curve; (b) stress-inelastic strain (input data in ABAQUS).
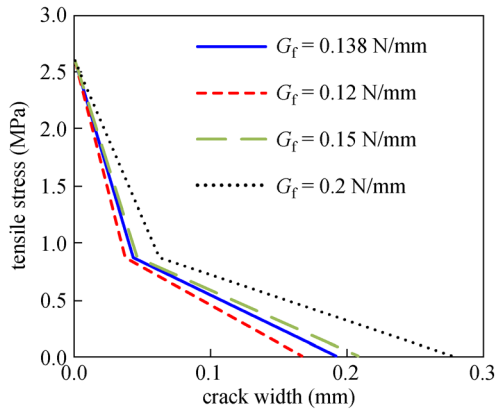
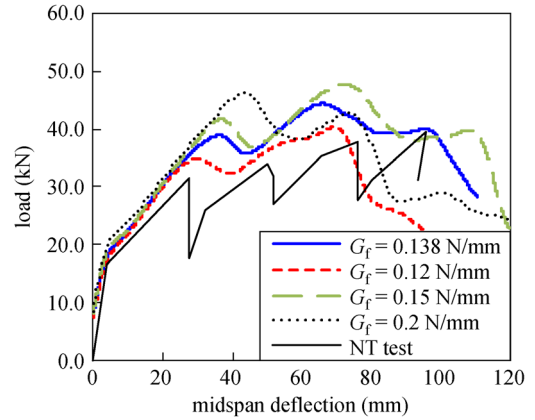**Fig. 6**   Tensile stress-crack width curves for the beam NT.

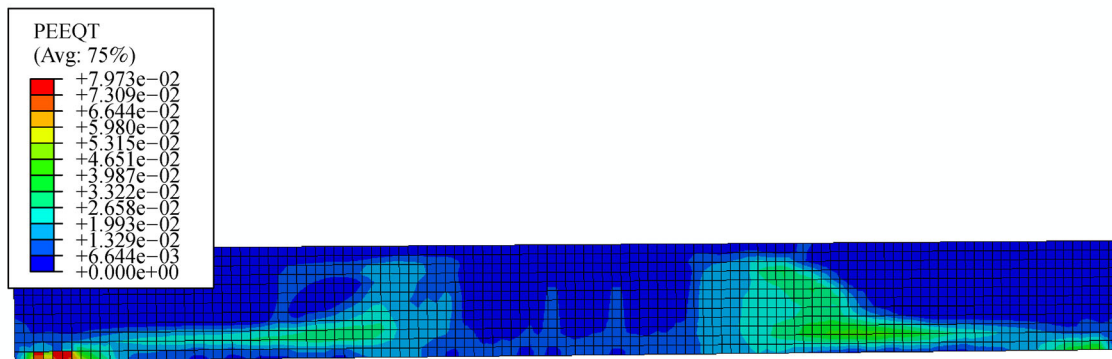**Fig. 7**   Load-deflection response curves for the beam NT: Fracture energy investigation.

Fig. 8   PEEQT tensile equivalent plastic strains representing cracking for the beam NT at failure.

the simplest remedies is the Crack Band Method that uses energy-based scaling of the softening portion of the stress-strain relationship [27]. This method is simple and effective and has been implemented in many concrete damage-plasticity models [28,29]. The concrete damaged plasticity model considered in this study uses the fracture energy-based regularization to describe the softening in tension and compression. The crack length can be calculated from the geometry and formation of the element, which is the length of a line across an element (first-order elements). Three different mesh sizes (20, 25, and 30 mm) were considered for the mesh sensitivity analysis. These values were chosen in order for the elements to be larger than the aggregate size (19 mm) and also to not result in coarse mesh. To avoid mesh size dependent results, the tensile cracking displacements were divided to the characteristic lengths of the elements (Fig. 9). Figure 10 shows the load-deflection responses for the three different mesh sizes and as it can be seen these results are mesh size dependent. Thus, the regularized tensile concrete model does not resolve the mesh sensitivity of the current problem.
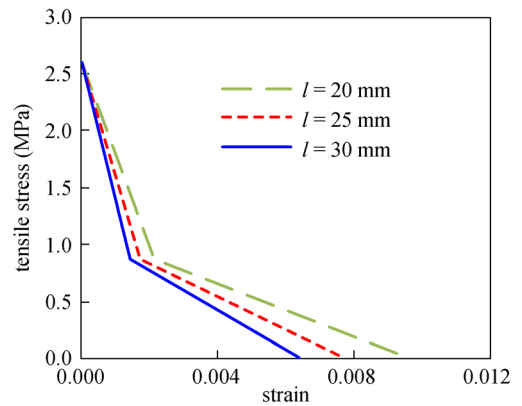
To further examine ways to overcome the mesh

Fig. 9   Regularized tensile stress-strain curves for the beam NT for $G_f = 0.138$ N/mm: mesh size investigation.

sensitivity problem, regularization was also considered for the compressive behavior of concrete, thus, both fracture and crushing energies are scaled in relation to the finite element size. Experimental observations [30–32] showed strain localization in compression and analytical investigation [33] indicated that the idea of fracture energy
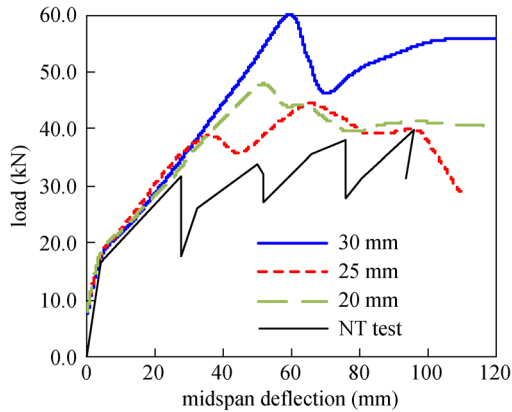
Fig. 10 Load-deflection response curves for the beam NT for G_f = 0.138 N/mm: mesh size investigation.

Fig. 12 Regularized compressive stress-strain curves for the beam NT for G_{fc} = 80 N/mm: mesh size investigation.

in tension can be also considered in compression [34]. Nakamura and Higai [35] defined the crushing energy of concrete to be related to its compressive strength and suggested a crushing energy of 80 N/mm for normal-weight unconfined concrete, as such 80 N/mm was chosen as the starting point for this investigation. Figure 11 shows the compressive stress versus plastic deformation graph considering the crushing energy equal to 80 N/mm. Then, similar to the regularized model in tension, the compressive stress-plastic deformation is converted to a stress versus strain curve by diving the plastic deformation with the characteristic length of the element (Fig. 12).
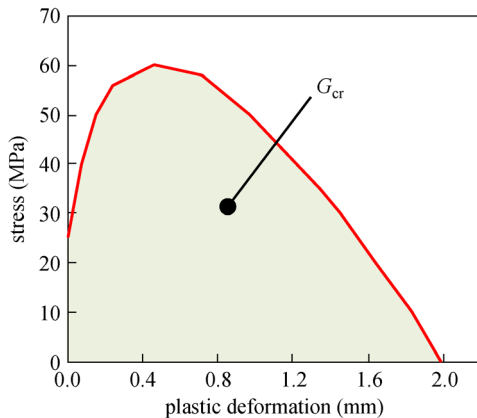

Fig. 13 Load-deflection response curves for the beam NT: mesh size investigation after material regularization.

mesh size of 25 mm is considered for all subsequent analyses. This mesh size is not too coarse, does converge and needs less computational time to run such an analysis. Figure 14 shows the cracking of beam NT with mesh size equal to 25 mm. The regularized concrete model in both tension and compression (Fig. 14) seems to presents in a more accurate manner the cracking compared to the crack patter of the real tested beam NT (Fig. 4).

3.2 FEA of beams with transverse reinforcement

To analyze the BFRP concrete beams with transverse reinforcement (BFRP stirrups) the calibrated regularized concrete model of the beam NT (no transverse reinforcement) is considered. During the test, beam FT achieved its peak load and then immediately the BFRP stirrups ruptured near their corners. Beam FC showed a similar response however first the concrete in the compression zone of the shear crack crushed at the peak load followed by the rupture of the stirrups.

The modeling of the stirrups was done using truss

Fig. 11 Compressive stress-plastic deformation for the beam NT considering crushing energy (G_{fc} = 80 N/mm).

Figure 13 demonstrates the load versus mid-span deflection for three different mesh sizes using the regularized concrete model for both tension and compression. The FEA results show that the mesh size sensitivity of the model has been improved. However, differences still remain when the first major shear crack appears and before the failure. To continue the investigation of the modeling parameters of the shear reinforced concrete beams, the
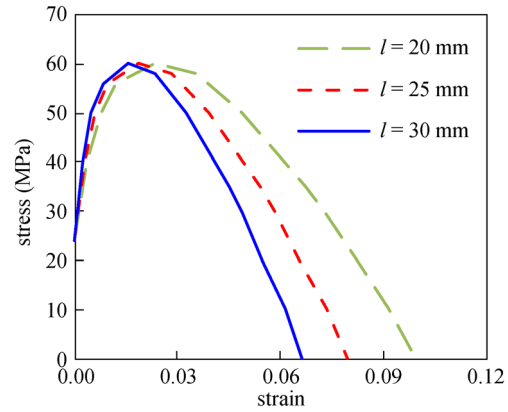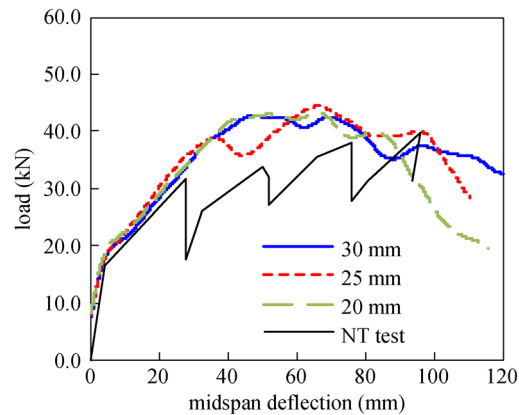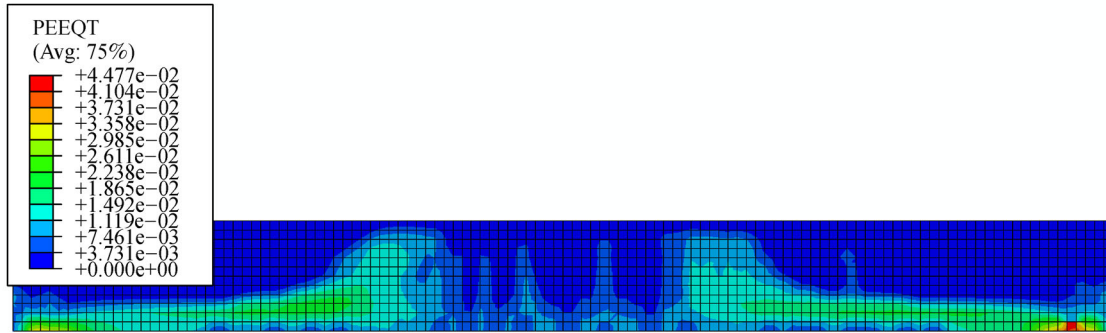
Fig. 14 PEEQT tensile equivalent plastic strains representing cracking for the beam NT at failure: $G_f = 0.138$ N/mm, $G_{fc} = 80$ N/mm, mesh size = 25 mm.

elements similar to the longitudinal reinforcement. However, these elements can carry only axial loading and the analysis of the beams FT and FC using the calibrated model did not demonstrate the influence of stirrups to the load capacity of the beams. Thus, to account for the confinement provided by the BFRP stirrups the dilation angle of the CDP model was increased.

Concrete undergoes significant volume change, called dilatancy, caused by inelastic strains. In the CDP model this dilatancy is defined by specifying the dilation angle. The dilation angle of concrete is considered as a material parameter that depends on the strength of concrete and its confinement in the case of reinforced concrete members. The ABAQUS manual considers a dilation angle equal to 36.3° for simulating a reinforced concrete dam. The value of the dilation angle used for the beam NT (no stirrups) was equal to 36° and herein, this value is increased to 40° after investigation to model the concrete beams with the BFRP stirrups. The FEA results in terms of load versus mid-span deflection are shown in Fig. 15. Figure 16 demonstrates the maximum principal plastic strains that represent the cracking.
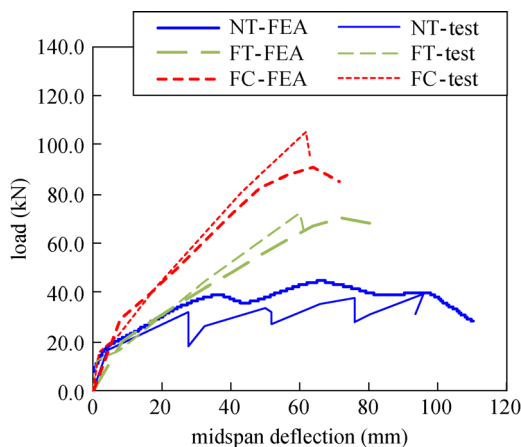

Fig. 15 Load-deflection curves of the beams.

Cracking of beams FC and FT appeared different compared to specimen NT (no stirrups) since the rupture of stirrups is shown. Beam FT showed rupture of stirrups at the ultimate load, while beam FC showed first crushing in the compression zone of the shear crack at the peak load and then rupture in the stirrups. In all comparisons between FEA and test results in terms of loads and displacements, the relative error was within 10%. This is an accepted difference and of course can be explained in many ways, with the most possible to be the pre-cracking (e.g., shrinkage, handling) of the specimens prior to tests. Table 4 in Section 4 summarizes the failure loads of the tested and analyzed beams.

4 Design codes

Test and numerical results were compared to the predicted loads of CSA S806-12 and ACI 440.1R-15. A description of the design equations with explanation of all parameters is given. CSA S806-12 suggests that the total factored shear capacity (V_R) of a beam, is a contribution of the factored resistance provided by concrete (V_c) and the factored shear resistance provided by FRP stirrups (V_{SF}). The upper limit of the ultimate shear resistance is given in Eq. (3):

$$V_R \leqslant V_{R,\max} = 0.22\varphi_c f_c' b_w d_v, \qquad (3)$$

where φ_c is the safety factor of concrete, f_c' is the compressive strength of concrete, b_w is the depth of beam, and d_v is the effective shear depth. The effective shear depth is taken to be larger of $0.9d$ or $0.72h$, where d is the effective depth and h is the height of the beam. The contribution of concrete to the shear capacity of beams with an effective depth less than 300 mm and f_c' less than 60 MPa is given in Eq. (4):

$$V_c = 0.005\lambda\varphi_c k_m k_r (f_c')^{1/3} b_w d_v, \qquad (4)$$

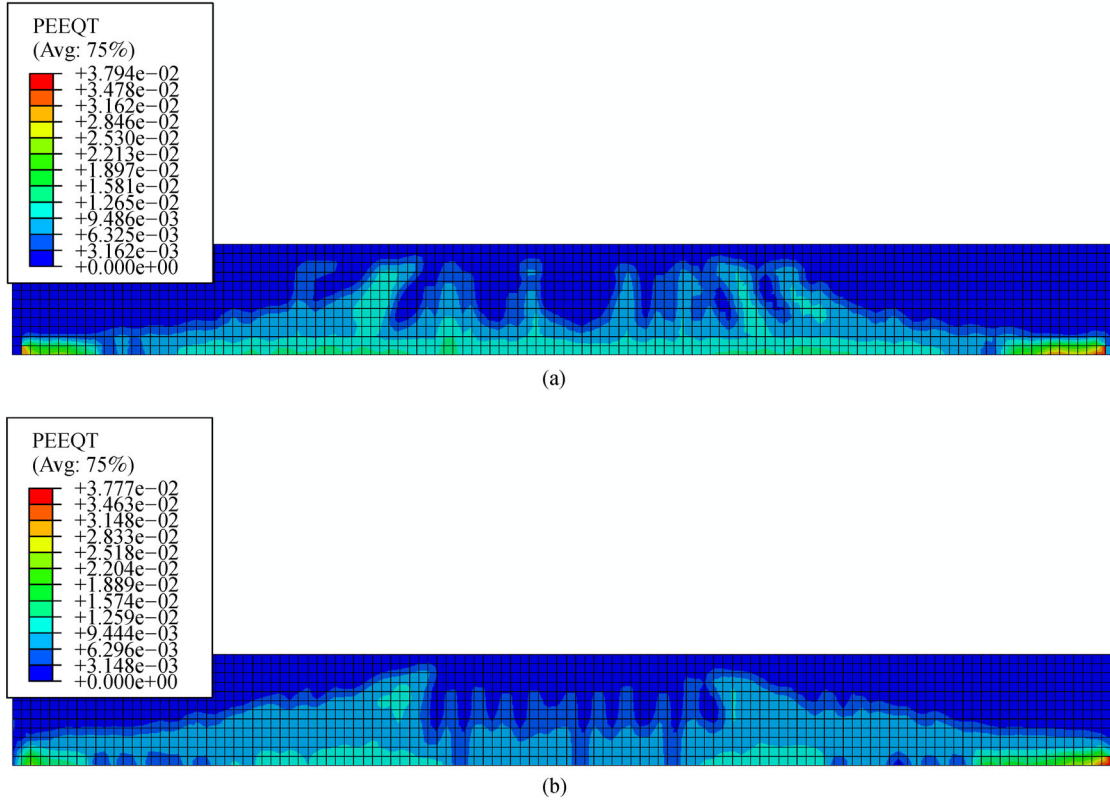where λ is a factor that is taken equal to 1 for normal

Fig. 16 PEEQT tensile equivalent plastic strains representing cracking at failure for beams: (a) FC and (b) FT.

density concrete, k_m is a factor that accounts for the bending moment, and k_r is a factor that accounts for the reinforcement's rigidity. Equations (5) and (6) calculate the factors k_m and k_r as follow:

$$k_m = \sqrt{\frac{V_f d}{M_f}} \leqslant 1.0, \tag{5}$$

$$k_r = 1 + (E_f \rho_{Fw})^{1/3}, \tag{6}$$

where V_f and M_f are the factored shear force and bending moment respectively, E_f is the Young's Modulus of BFRP bars, and ρ_{Fw} is the flexural reinforcement ratio. V_c shall not be taken greater than $0.22\varphi_c \sqrt{f'_c} b_w d_v$ nor less than $0.11\varphi_c \sqrt{f'_c} b_w d_v$.

For beams with transverse reinforcement perpendicular to the longitudinal axis the factored shear resistance provided by FRP stirrups V_{SF} is calculated according to Eq. (7):

$$V_{SF} = \frac{0.4\varphi_F A_{Fv} f_{Fu} d_v}{s} \cot\theta, \tag{7}$$

where φ_F is the safety factor for FRP, A_{Fv} is the area of transverse shear reinforcement, f_{Fu} is the ultimate tensile strength of FRP that shall not be greater than $0.005E_F$, s is the spacing of the shear reinforcement and the angle θ of

the diagonal compressive stress shall be calculated as:

$$\theta = 30° + 7000\varepsilon_1. \tag{8}$$

The angle θ shall not be taken greater than $60°$ nor less than $30°$. In Eq. (8), ε_1 is the longitudinal strain at mid-depth of the section that shall be calculated according to Eq. (9) and should be greater or equal to zero:

$$\varepsilon_1 = \frac{\frac{M_f}{d_v} + V_f}{2E_F A_f} \geqslant 0. \tag{9}$$

ACI 440.1R-15 suggests that the nominal shear strength V_n of a reinforced concrete beam, is the sum of the shear resistance provided by concrete V_c and the shear resistance provided by FRP stirrups V_f. The concrete shear capacity V_c is calculated according to Eq. (10):

$$V_c = \frac{2}{5}\sqrt{f'_c} b_w (kd), \tag{10}$$

where k is given by:

$$k = \sqrt{2\rho_f n_f + (\rho_f n_f)^2} - \rho_f n_f, \tag{11}$$

where ρ_f is the longitudinal FRP reinforcement ratio and n_f is the ratio of the modulus of elasticity of the longitudinal FRP reinforcement (E_f) to the modulus of the elasticity of

concrete (E_c). The shear resistance provided by the FRP stirrups is calculated according to Eq. (12):

$$V_f = \frac{A_{fv} f_{fv} d}{s},$$ (12)

where A_{fv} is the area of transverse shear reinforcement, f_{fv} is the ultimate tensile strength of FRP that shall be equal to $0.005 E_f$ and not greater to the tensile strength of the bent portion of the FRP stirrup, and is the spacing of the shear reinforcement.

Table 5 compares the test and FEA failure loads for the analyzed BFRP beams to the predicted loads of CSA S806-12 and ACI 440.1R-15. The predicted loads of the design codes did not consider the safety factors. CSA S806-12 equations seem to overestimate the shear strength of the beams NT and FT. CSA S806-12 code gives safe predictions only for the beam FC that has stirrups and increased flexural reinforcement ratio compared to the beam FT. ACI 440.1R-15 in all cases underestimates the strength of the beams providing safe predictions.

Table 5 Comparison between test, numerical, and design codes failure loads

beam	test failure load (kN) [30]	FEA failure load (kN)	CSA S806-12 (kN)	ACI 440.1 R-15 (kN)
NT	41.8	44.5	62.1	28.1
FT	72.7	69.6	89.8	64.7
FC	106.9	96.5	82.2	76.6

5   Conclusions

Three-dimensional FEA can be considered to examine the response of BFRP reinforced concrete beams with the main objective to supplement the experimental data and perform parametric studies to better understand their behavior. However, FEA require much time, effort, and attention due to the complex constitutive concrete model. To verify the capability of the FEA model first consideration should always be the calibration with test results. In this paper, the concrete damaged plasticity model in ABAQUS software was used to analyze three previously tested BFRP reinforced concrete beams. Test and numerical results were compared to the current design provisions (CSA S806-12 and ACI 440.1R-15). The study focused on a detailed description and justification of the calibration process considering different material and model parameters. The following conclusions are offered:

1) The calibration of the concrete model was done based on the response of the beam NT (beam without stirrups), where the most critical part in the calibration process was to avoid the mesh sensitivity. The results showed that the fracture energy and the characteristic length did not provide a good mesh objective load-deflection response, unless the crushing energy was considered to regularize the concrete model. This mesh-size independent model provided in this study potentially can be further improved using the viscoplastic rate-dependent regularization.

2) The effect of the BFRP stirrups in beams FC and FT was shown in the numerical simulations after considering further calibration to achieve the confinement that the stirrups provided in the real tests. Increased dilation angle was adopted in this study and was capable to model the confined beams since their results were in good agreement with the test results.

3) Test and FEA results in terms of load-deflection response and crack patterns were in good agreement indicating the effectiveness of the calibrated concrete damaged plasticity model in ABAQUS to accurately predict the response of the BFRP beams. Future parametric studies can address different aspects of the response of the BFRP beams.

4) Finally, test and FEA shear strengths were compared to CSA S806-12 and ACI 440.1R-15. CSA S806-12 seems to overestimate the shear strength of the beams NT and FT but it gives safe predictions for the beam FC. ACI 440.1R-15 seems to underestimate the strength of the beams providing safe predictions.

BFRP reinforced concrete beams can be used in practice together with the other types of FRP reinforced concrete beams. Future studies will provide improved FEA models including the bond-slip behavior between BFRP reinforcing bars and concrete with the objective to perform parametric studies and propose modifications to the current design provisions. Future study aims to examine more design provisions and strength prediction methods for FRP reinforced concrete beams.

References

1. American Concrete Institute (ACI). Guide for the Design and Construction of Structural Concrete Reinforced with Fiber-Reinforced Polymer (FRP) Bars, ACI 440.1R–15. Farmington Hills, MI: ACI Committee 440, 2015

2. Ross A. Basalt fibers: Alternative to glass. Component Technology, 2006, 12(4): 44–48

3. Urbanski M, Lapko A, Garbacz A. Investigation on concrete beams reinforced with basalt rebars as an effective alternative of conventional R/C structures. Procedia Engineering, 2013, 57 (Supplement C): 1183–1191

4. Tomlinson D, Fam A. Performance of concrete beams reinforced with basalt FRP for flexure and shear. Journal of Composites for Construction, 2015, 19(2): 04014036

5. El Refai A, Abed F. Concrete contribution to shear strength of beams reinforced with basalt fiber-reinforced bars. Journal of Composites for Construction, 2015, 20(4): 1–13

6. Issa M A, Ovitigala T, Ibrahim M. Shear behavior of basalt fiber reinforced concrete beams with and without basalt FRP stirrups. Journal of Composites for Construction, 2016, 20(4): 04015083

7. Dassault Systems Simulia Corp. ABAQUS Analysis User'S Manual 6.12-3. 2012

8. Hillerborg A, Modéer M, Petersson P E. Analysis of crack formation and crack growth in concrete by means of fracture mechanics and finite elements. Cement and Concrete Research, 1976, 6(6): 773–781

9. Canadian Standards Association (CSA). Design and Construction of Building Structures with Fibre-Reinforced Polymers, S806-12. Mississauga, ON: CSA Group, 2012

10. European Committee for Concrete. CEB-FIP-model Code 1990: Design Code. London: Thomas Telford, 1993

11. Pramono E, Willam K. Fracture energy-based plasticity formulation of plain concrete. Journal of Engineering Mechanics, 1989, 115(6): 1183–1204

12. Imran I, Pantazopoulou S J. Plasticity model for concrete under triaxial compression. Journal of Engineering Mechanics, 2001, 127(3): 281–290

13. Grassl P, Lundgren K, Gylltoft K. Concrete in compression: A plasticity theory with a novel hardening law. International Journal of Solids and Structures, 2002, 39(20): 5205–5223

14. Kachanov L M. Introduction to Continuum Damage Mechanics. Dordrecht: Martinus Nijhoff Publishers, 1986

15. Mazars J. A model of unilateral elastic damageable material and its application to concrete. In: Wittmann F H, ed. Fracture Toughness and Fracture Energy of Concrete. Amsterdam: Elsevier Science Publishers, 1986, 61–71

16. Mazars J, Pijaudier-Cabot G. Continuum damage theory-application to concrete. Journal of Engineering Mechanics, 1989, 115(2): 345–365

17. Lemaitre J, Chaboche J L. Mechanics of Solid Materials. New York: Cambridge University Press, 1990

18. Simo J C, Ju J W. Strain- and stress- based continuum damage models-I. Formulation. International Journal of Solids and Structures, 1987, 23(7): 821–840

19. Simo J C, Ju J W. Strain- and stress-based continuum damage model-II. Computational aspects. International Journal of Solids and Structures, 1987, 23(7): 841–869

20. Ju J W. On energy-based coupled elastoplastic damage theories: Constitutive modeling and computational aspects. International Journal of Solids and Structures, 1989, 25(7): 803–833

21. Lubliner J, Oliver J, Oller S, Oñate E. A plastic-damage model for concrete. International Journal of Solids and Structures, 1989, 25(3): 299–326

22. Lee J, Fenves G L. Plastic-damage model for cyclic loading of concrete structures. Journal of Engineering Mechanics, 1998, 124(8): 892–900

23. Genikomsou A S, Polak M A. Finite element analysis of punching shear of concrete slabs using damaged plasticity model in ABAQUS. Engineering Structures, 2015, 98(4): 38–48

24. Hillerborg A. The theoretical basis of a method to determine the fracture energy G_F of concrete. Materials and Structures, 1985, 18(4): 291–296

25. Scanlon A. Time dependent deflections of reinforced concrete slabs. Dissertation for the Doctoral Degree. Edmonton: University of Alberta, 1971

26. Bergan P G, Holand I. Nonlinear finite element analysis of concrete structures. Computer Methods in Applied Mechanics and Engineering, 1979, 17–18: 443–467

27. Bažant Z, Oh B. Crack band theory for fracture of concrete. Materials and Structures, 1983, 16(3): 155–177

28. Grassl P, Jirásek M. Damage-plastic model for concrete failure. International Journal of Solids and Structures, 2006, 43(22–23): 7166–7196

29. Cicekli U, Voyiadjis G, Abu Al-Rub R. A plasticity and anisotropic damage model for plain concrete. International Journal of Plasticity, 2007, 23(10–11): 1874–1900

30. Kotsovos M D. Effect of testing techniques on the post-ultimate behavior of concrete in compression. Materials and Structures, 1983, 16(1): 3–12

31. Van Mier J G M. Strain-Softening of Concrete under Multiaxial Loading Conditions. Eindhoven: Eindhoven University of Technology, 1984

32. Jansen D C, Shah S P. Effect of length on compressive strain softening of concrete. Journal of Engineering Mechanics, 1997, 123(1): 25–35

33. Markeset G, Hillerborg A. Softening of concrete in compression—Localization and size effects. Cement and Concrete Research, 1995, 25(4): 702–708

34. Van Mier J G M. Concrete Fracture: A Multiscale Approach. New York: CRC Press, 2012

35. Nakamura H, Higai T. Compressive Fracture Energy and Fracture Zone Length of Concrete. Reston, VA: ASCE, 2001